AN EFFICIENT FEM-SFEM ITERATIVE COUPLING PROCEDURE FOR ELASTODYNAMIC PROBLEMS

Jonathan E. Arroyo Silva[a] **and Felipe dos Santos Loureiro**[b]

[a]*Postgraduate Program in Computational Modeling, Federal University of Juiz de Fora, Juiz de Fora, Minas Gerais, Brazil, http://www.ufjf.br/pgmc*

[b]*Department of Thermal and Fluid Sciences, Federal University of São João del-Rei, São João del-Rei, Minas Gerais, Brazil, http://http://www.ufsj.edu.br*

Keywords: FEM, spectral FEM, iterative coupling, elastodynamic.

Abstract. In the present work, an efficient iterative coupling methodology between the Finite Element Method (FEM) and the Spectral Finite Element Method (SFEM) for the modeling of elastodynamic problems in the time domain is presented. The methodology allows the use of a nonconforming mesh at the interface between the subdomains, as well as independent time-step sizes within each subdomain. By minimizing a square error functional, an adaptive strategy for the relaxation parameter can be established in the iterative process, increasing the efficiency of the FEM-SFEM coupled analysis. Numerical simulations are presented in order to illustrate the accuracy and potentialities of the proposed methodology.

1   INTRODUCTION

The finite element method (FEM) and the Spectral Finite Element Method (SFEM) are widely used for the numerical solution of partial differential equations in many fields of engineering and computational modeling (Bathe, 1996; Hughes, 2000; Komatitsch and Tromp, 1999; Canuto et al., 2006). The latter can be treated as a high-order FEM formulation, therefore, allowing to get the same accuracy as the FEM when using a reduced number of grid points, thus giving rise to a significant save of computational resources (Komatitsch and Vilotte, 1998).

It is well-know that the SFEM presents loss of accuracy when dealing with complicated geometries (Canuto et al., 2007). In this sense, the FEM-SFEM coupling intends to take advantage of both the methods, using the SFEM in the subdomain with simple geometries, saving computational resources, and the FEM in the complicated geometries subdomain, resulting in precise numerical solutions.

Thus, interface coupling iterative procedures appear as an attractive way to handle the aforementioned issue, once each subdomain is analyzed separately (resulting in well-conditioned systems). Hence, only the information on the coupling interface needs to be transferred through the subdomains iteratively until attain the desired precision, not being required matching meshes at the coupling interface (Elleithy et al., 2001; Jr et al., 2015). Therefore, some numerical advantages like sparse matrix storage or iterative solvers may be preserved.

In this work an efficient iterative multi-time-step coupling methodology between the FEM-SFEM for the modeling of elastodynamic problems in the time domain is presented. A numerical example is presented in order to illustrate the accuracy of the methodology.

2   FEM/SFEM FOR ELASTODYNAMIC PROBLEMS

Elastodynamic problems are mathematically modeled as next: Let $\Omega = \bigcup \Omega_k \subset \mathbb{R}^d$ be a bounded domain, where d is the number of spatial dimensions of the problem under consideration with k being related with the number of the subdomains, and $I = (0, T] \subset \mathbb{R}^+$ been the time domain of the analysis. Thereby:

$$\rho^k \ddot{u}_i^k - \sigma_{ij,j}^k = b_i^k \text{ in } \Omega_k \times I \tag{1}$$

is the traditional elastodynamic equation, where $u_i^k : \Omega_k \times I \to \mathbb{R}$, $b_i^k : \Omega_k \times I \to \mathbb{R}$ and $\sigma_{ij}^k : \Omega_k \times I \to \mathbb{R}$ stand, respectively, for the displacements, given body force per unit volume and Cauchy stress tensor components; and $\rho^k : \Omega_k \to \mathbb{R}^+$ is the mass density related to each subdomain Ω_k.

Moreover, considering the boundary partition $\partial \Omega_k = \Gamma_k = \Gamma_{k,D_i} \cup \Gamma_{k,N_i}$ with $\Gamma_{k,D_i} \cap \Gamma_{k,N_i} = \emptyset$, the boundary conditions are given by:

$$u_i^k = \bar{u}_i^k \text{ on } \Gamma_{k,D_i} \times I, \ \ \tau_i^k \equiv \sigma_{ij}^k n_j^k = \bar{\tau}_i^k \text{ on } \Gamma_{k,N_i} \times I$$

where $\bar{u}_i^k : \Gamma_{k,D_i} \times I \to \mathbb{R}$ are prescribed displacements, $\bar{\tau}_i^k : \Gamma_{k,N_i} \times I \to \mathbb{R}$ are prescribed traction and n_j^k being the outward normal vector components on Γ_{k,N_i}. Finally, the stress-strain relation is considered to be linear and isotropic (Bathe, 1996).

2.1   Spectral elements

In a similar way to that in the FEM, in the SFEM formulation, the subdomain Ω_k is also partitioned into nel nonoverlapping elements Ω_{k_n}, i.e., $\Omega_k^h = \cup_{n=1}^{nel} \Omega_{k_n}$ and $\Omega_{k_n} \cap_{\forall n \neq n'} \Omega_{k_{n'}} = \emptyset$. Hence, there is a diffeomorphism that preserves the orientation called mapping function, defined

as $\mathcal{F} : \Lambda \to \Omega_{k_n}$, which relates each element Ω_{k_n} with the reference closed element domain Λ; in this case a biunitary square $\Lambda = [-1, 1]^2$.

Defining $\mathbf{S}_k^h \subset \mathbf{S}_k$ and $\mathbf{V}_k^h \subset \mathbf{V}_k$ to be the finite element spaces (related with the h superscript) of admissible solutions and the test functions (Hughes, 2000), respectively, and $\mathbb{P}(\Lambda)$ to be the space generated by the tensor product of the Lagrange polynomials with degree $\leq m$, we have:

$$\mathbf{S}_k^h = \left\{ p_i^{k,h} \mid p_i^{k,h}(\cdot, t) \in H^1(\Omega_k), p_i^{k,h} = \bar{p}_i^{k,h} \text{ on } \Gamma_{k,D_i} \times I \right.$$
$$\left. \text{and } p_i^{k,h}|_{\Omega_{k_n}} \circ \mathcal{F} \in \mathbb{P}(\Lambda) \right\}$$

$$\mathbf{V}_k^h = \left\{ w_i^{k,h} \mid w_i^{k,h} \in H^1(\Omega_k), w_i^{k,h} = 0 \text{ on } \Gamma_{k,D_i} \right.$$
$$\left. \text{and } w_i^{k,h}|_{\Omega_{k_n}} \circ \mathcal{F} \in \mathbb{P}(\Lambda) \right\}$$

where H^1 is the classical Sobolev space that denotes the space of square-integrable functions with square-integrable generalized first derivatives (Adams and Fournier, 2003).

In a different way to that the standard high-order FEM with degree m (with internal equidistant nodal distributions), in the SFEM, the local nodal points are obtained by the tensor product of the $m + 1$ Gauss-Lobatto-Legendre (GLL) points localized in the interval $[-1, 1]$, defined as the roots of the equation $\frac{\partial P_m}{\partial \xi}(\xi^2 - 1) = 0$, in which P_m is the mth Legendre polynomial and resulting in $(m + 1)^2$ points for the case when are used quadrilaterals elements in the bidimensional case (i.e., when $d = 2$) (Komatitsch and Vilotte, 1998; Komatitsch and Tromp, 1999), as one can see in the Fig. 1, where are illustrated some quadrilateral spectral finite elements according to the degree m.
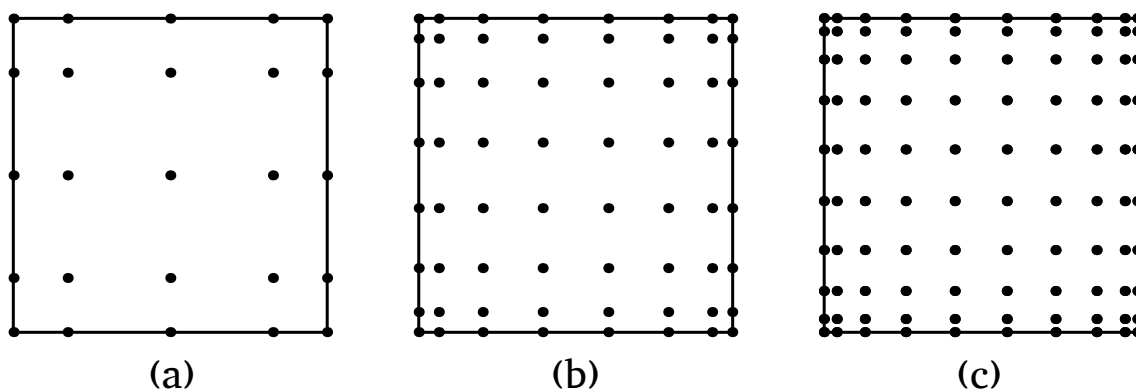

Figure 1: 2D spectral elements with degree m: (a) 4×4; (b) 7×7; (c) 9×9.

In the same way, the local interpolation functions N_i^e in Λ are obtained by the tensor product of the Lagrange polynomials of degree m using the $m + 1$ GLL points (previously introduced) in each direction with the relation $N_i^e(\boldsymbol{\xi}_j) = \delta_{ij}$, $i, j = 1, \dots, (m + 1)^2$, where δ_{ij} is the Kronecker delta operator.

At the same time, a quadrature rule based on the tensor product of the unidimensional GLL formulae is used (Canuto et al., 2006), here, the weights $\omega_{i,m}$ and corresponding quadrature points are defined, respectively, as $\omega_{i,m} = \frac{2}{m(m+1)} \frac{1}{P_m(\xi_i)}$ and ξ_i. Such quadrature points coincide with the GLL points also adopted in the interpolation functions, leading to a degree of precision $\leq 2m - 1$.

2.2   Time-stepping technique

By means of the semi-discrete FEM and SFEM formulation where the spatial domain is discretized independently of the time domain, the following ODE system is obtained (Bathe, 1996):

$$\mathbf{M}_k \ddot{\mathbf{U}}_k + \mathbf{K}_k \mathbf{U}_k = \mathbf{F}_k \tag{2}$$

where $\mathbf{M}_k \in \mathbb{R}^{nq_k \times nq_k}$ and $\mathbf{K}_k \in \mathbb{R}^{nq_k \times nq_k}$ denote the standard mass and stiffness matrices respectively, the vectors $\mathbf{U}_k : I \to \mathbb{R}^{nq_k}$, $\ddot{\mathbf{U}}_k : I \to \mathbb{R}^{nq_k}$, $\mathbf{F}_k : I \to \mathbb{R}^{nq_k}$ represent, respectively, the nodal displacements, accelerations and external forces with nq_k being the number of equations related with each the subdomain Ω_k.

In this work, the analysis time I is partitioned into L_k equal time subintervals (related with each the Ω_k subdomains, allowing a better time-domain modelling for each sub-domain), i.e., $[0, T] = \cup_{l=0}^{L_k-1} [t_{k,l}, t_{k,l+1}]$, with $0 < t_{k,0} < \ldots < t_{k,L_k} = T$, $\Delta t_k = t_{k,l+1} - t_{k,l} = T/L_k$ and $t_{k,l+1} = (l+1)\Delta t_k$ so that $\mathbf{U}_k^{l+1} = \mathbf{U}_k(t_{k,l+1})$. Then the Newmark *a-form* is implemented as follows (Hughes, 2000):

$$\mathbf{M}_k \ddot{\mathbf{U}}_k^{l+1} + \mathbf{K}_k \mathbf{U}_k^{l+1} = \mathbf{F}_k^{l+1}$$

$$\mathbf{U}_k^{l+1} = \mathbf{U}_k^l + \Delta t_k \dot{\mathbf{U}}_k^l + \frac{\Delta t_k^2}{2} \left[(1 - 2\beta) \ddot{\mathbf{U}}_k^l + 2\beta \ddot{\mathbf{U}}_k^{l+1} \right] \tag{3}$$

$$\dot{\mathbf{U}}_k^{l+1} = \dot{\mathbf{U}}_k^l + \Delta t_k \left[(1 - \gamma) \ddot{\mathbf{U}}_k^l + \gamma \ddot{\mathbf{U}}_k^{l+1} \right]$$

followed by a *predictor-corrector* scheme, in the velocity and displacements nodal vectors as next:

$$\tilde{\mathbf{U}}_k^{l+1} = \mathbf{U}_k^l + \Delta t_k \dot{\mathbf{U}}_k^l + \frac{\Delta t_k^2}{2}(1 - 2\beta)\ddot{\mathbf{U}}_k^l$$

$$\tilde{\dot{\mathbf{U}}}_k^{l+1} = \dot{\mathbf{U}}_k^l + (1 - \gamma)\Delta t_k \ddot{\mathbf{U}}_k^l \tag{4}$$

Equation (3) may then be written as:

$$(\mathbf{M}_k + \beta \Delta t_k^2 \mathbf{K}_k)\ddot{\mathbf{U}}_k^{l+1} = \mathbf{F}_k^{l+1} - \mathbf{K}_k \tilde{\mathbf{U}}_k^{l+1}$$

$$\mathbf{U}_k^{l+1} = \tilde{\mathbf{U}}_k^{l+1} + \beta \Delta t_k^2 \ddot{\mathbf{U}}_k^{l+1} \tag{5}$$

$$\dot{\mathbf{U}}_k^{l+1} = \tilde{\dot{\mathbf{U}}}_k^{l+1} + \gamma \Delta t_k \ddot{\mathbf{U}}_k^{l+1}$$

where, to start the time-marching process, $\ddot{\mathbf{U}}_k^0$ may be calculated from

$$\mathbf{M}_k \ddot{\mathbf{U}}_k^0 = \mathbf{F}_k^0 - \mathbf{K}_k \mathbf{U}_k^0 \tag{6}$$

Another point are the parameters γ and β, which determine the stability and accuracy characteristics of the algorithm under consideration.

3   ITERATIVE MULTI-TIME-STEP COUPLING METHOD

In the present section, the coupling procedure is explained in a simple way. For the coupled analysis in elastodynamic problems, the following continuity and equilibrium equations must hold for the interfaces between the FEM and SFEM sub-domains:

$$\begin{aligned} \bar{\mathbf{U}}_k^l &= \bar{\mathbf{U}}_{k'}^l \\ \mathbf{F}_k^l + \mathbf{F}_{k'}^l &= 0 \end{aligned} \quad ; k \neq k' \tag{7}$$

where the upper bar means the interface nodal values, and in order to obtain consistency between the FEM and the SFEM formulations, $\mathbf{F}_{k'}^{l}$ represents SFEM equivalent nodal forces that are obtained from the SFEM nodal traction vector by a pos-processing procedure. Additionally, in order to speedup the convergence of the methodology, a relaxation process is employed for the values of the variables at the coupling interface as discussed later on.

3.1 Non-conforming mesh at the coupling interface

In order to correctly approximate the nodal values at the coupling interface, an inverse mapping followed by an interpolation procedure are employed. This scheme is illustrated in Figure 2, notice that for the SFEM the GLL integration points coincide with the nodal points and one can use this in order to improve the accuracy of the results.
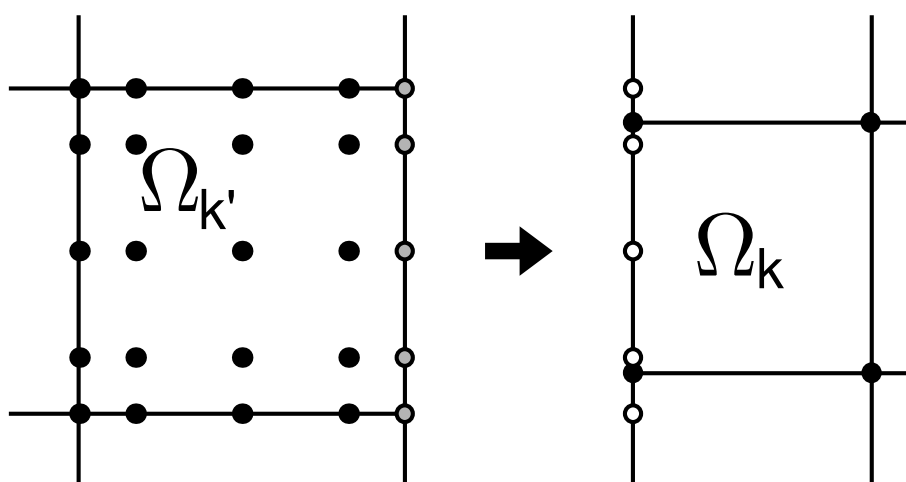

Figure 2: Sketch of the inverse mapping of the points; the inverse mapped points are represented by the void points, the black points represent the mesh nodes.

Once the points in the physical coupling boundary of $\Omega_{k'}$ are known (gray points), the corresponding element on Ω_k is readily identified, and an inverse mapping procedure in the element Ω_k enables us to compute the interpolated displacement values at the void nodes, using naturally, the FEM interpolation function.

When the inverse mapping is performed in the subdomain Ω_k instead the $\Omega_{k'}$, using a subparametric approximation for the SFEM (i.e., bilinear quadrilateral elements with interpolation functions of degree $m = 1$), the inverse mapping falls into the same case previously discussed. Although this subparametric approximation is adopted here, if a better representation of the geometry boundary is required, more complex mapping schemes could also be employed (e.g., blending or spline type functions) (Szabo and Babuška, 1991).

3.2 Time sub-cycling – different time steps

The difference between the time-step size at each sub-domain, is carried out by a interpolation/extrapolation scheme as follows: Considering $\Delta t_k \leq \Delta t_{k'}$, and assuming that $t_{k',l} < t_{k,l+1} < t_{k',l+1}$:

- $\bar{\mathbf{U}}_{k}^{l+1,h+1}$ extrapolation:
  - A constant time-extrapolation for the displacement nodal values of the current iterative step $h + 1$ is used, yielding $\bar{\mathbf{U}}_{k'}^{l+1,h+1} = \bar{\mathbf{U}}_{k}^{l+1,h+1}$

- $\bar{\mathbf{U}}_{k'}^{l+1,h+1}$ interpolation:

  – The displacement nodal values, already obtained, are linearly time-interpolated between the values of the previous time step $\bar{\mathbf{U}}_{k'}^{l}$ and those of the current iterative step at the current time step, i.e. $\bar{\mathbf{U}}_{k}^{l+1,h+1} = (1-\varepsilon)\bar{\mathbf{U}}_{k'}^{l} + \varepsilon\bar{\mathbf{U}}_{k'}^{l+1,h+1}$, where $\varepsilon = \dfrac{t_{k,l+1} - t_{k',l}}{\Delta t_{k'}}$.

3.3 Optimal relaxation parameter

In order to enhance and/or speedup the convergence of the iterative procedure, a relaxation parameter namely λ is adopted in the computation of the relevant variables at the coupling interface.

In this work, an optimal value for the relaxation parameter for each iterative step is computed based on the minimization of the square error functional of the displacements at the coupling interface (i.e., $\bar{\mathbf{U}}_k$) of one of the subdomains Ω_k (Elleithy et al., 2001; Jr et al., 2015). More precisely, the square error functional concerning the displacements in the time step $l+1$ between two successive iterative steps $h+1$ and h is considered (h here is referred to the iterative step), namely:

$$\mathcal{L}(\lambda) = \|\bar{\mathbf{U}}_k^{l+1,h+1} - \bar{\mathbf{U}}_k^{l+1,h}\|^2 \tag{8}$$

where $\bar{\mathbf{U}}_k^{l+1,h+1} = \lambda\bar{\mathbf{U}}_k^{l+1,h+\lambda} + (1-\lambda)\bar{\mathbf{U}}_k^{l+1,h}$ and $\bar{\mathbf{U}}_k^{l+1,h} = \lambda\bar{\mathbf{U}}_k^{l+1,h+\lambda-1} + (1-\lambda)\bar{\mathbf{U}}_k^{l+1,h-1}$ are the relaxed displacements, and $\bar{\mathbf{U}}_k^{l+1,h+\lambda}$; $\bar{\mathbf{U}}_k^{l+1,h+\lambda-1}$ the non-relaxed displacements, giving:

$$\begin{aligned}\mathcal{L}(\lambda) &= \|\lambda\mathbf{W}^{h+\lambda} + (1-\lambda)\mathbf{W}^h\|^2 \\ &= \lambda^2\|\mathbf{W}^{h+\lambda}\|^2 + 2\lambda(1-\lambda)(\mathbf{W}^{h+\lambda}, \mathbf{W}^h) + (1-\lambda)^2\|\mathbf{W}^h\|^2\end{aligned} \tag{9}$$

where $(\mathbf{W}, \mathbf{W}) = \|\mathbf{W}\|^2$ and with the variables $\mathbf{W}^{h+\lambda} = \bar{\mathbf{U}}_k^{l+1,h+\lambda} - \bar{\mathbf{U}}_k^{l+1,h+\lambda-1}$ and $\mathbf{W}^h = \bar{\mathbf{U}}_k^{l+1,h} - \bar{\mathbf{U}}_k^{l+1,h-1}$. Differentiating the functional with respect to λ and equating to zero, one obtains:

$$\lambda\|\mathbf{W}^{h+\lambda}\|^2 + (1-2\lambda)(\mathbf{W}^{h+\lambda}, \mathbf{W}^h) + (\lambda-1)\|\mathbf{W}^h\|^2 = 0 \tag{10}$$

and finally

$$\lambda = \frac{(\mathbf{W}^h, \mathbf{W}^h - \mathbf{W}^{h+\lambda})}{\|\mathbf{W}^h - \mathbf{W}^{h+\lambda}\|^2} \tag{11}$$

Notice that the obtained expression possesses a simple implementation and a low computational cost; and $\lambda = 0.5$, is employed at the first iteration step.

4 NUMERICAL EXAMPLE

In the numerical example, a partitioned elastic column is analyzed, and the sub-cycling scheme (different time-steps for each sub-domain) is used. For the Newmark time-marching scheme the constants are considered as $\gamma = 0.60$ and $\beta = 0.3$. Moreover, the tolerance used in the iterative coupling procedure for the relative errors is set to $\epsilon = 10^{-7}$.

The elastic column with dimensions $a = 4.0$m and $b = 1.0$m is subjected to a sinusoidal load $f(t) = \sin(\pi t)(H(t) - H(t - 1.0))$, acting at one of its ends, as depicted in Figure 3. As one can see, the Ω_1 subdomain is discretized by 4 spectral elements with degree $m = 7$, resulting in a total of 225 nodes, whereas the Ω_2 subdomain is discretized by 200 four-noded quadrilateral elements, resulting in 231 nodes. The material properties of the medium in both the subdomains
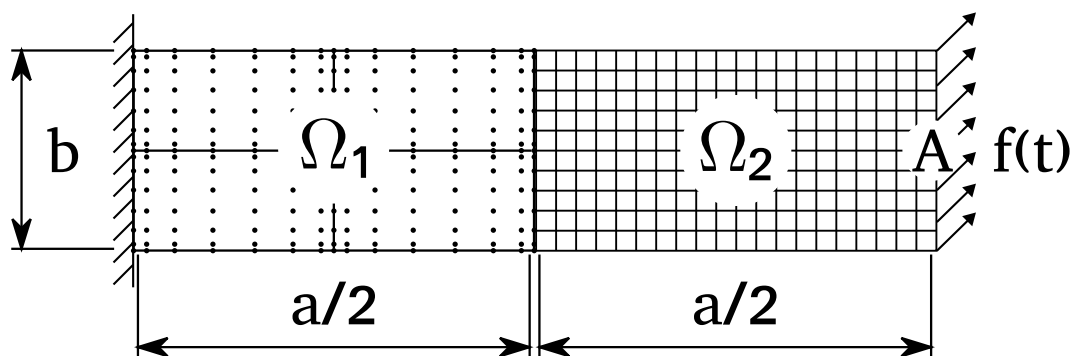
Figure 3: Elastic partitioned model and meshes.

are: $E = 10^2 \text{N/m}^2$ (Young modulus); $\nu = 0.25$ (Poisson ratio); $\rho = 1.0 \text{kg/m}^3$. A time-step size $\Delta t_1 = 2 \times 10^{-3}$ is adopted for the SFEM subdomain, while the time step size for the FEM subdomain is taken from this reference value.

In Figure 4, the y-displacements at point $A = (a, b/2)$ are presented and, as one can see the number of sub-cycling steps with the use of different time-step sizes for the subdomains apparently does not influence on the accuracy of the results.

In Figure 5, snapshots of $\|\mathbf{u}\|$ in two different time instants are presented. The results appear to satisfy the continuity restraints at the coupling interface quite well.

Figure 6(a) shows the number of iterations required to reach convergence at each time step versus the percentage in which each iteration number appears. As one can see, when $\Delta t_1 = \Delta t_2$ (blue bars), the number of iterations per time step is in its majority 2 and 3, i.e., only 2 or 3 iterations are required to attain convergence for each time step. Moreover, as the difference between the time-step sizes increases, the number of total iterations also increases, but as shown in Figs.6(a), when $\Delta t_1 = 5\Delta t_2$ (orange bars) 40% of the time-steps need just one iteration to converge, indicating the importance of a dynamic relaxation parameter.

Figure 6(b) shows the values of λ versus the percentage of appearance (computed throughout the whole iterative process in all the time steps). In the case of $\Delta t_1 = \Delta t_2$ (blue bars), the most appeared values are around $\lambda = 0.85$ and $\lambda = 0.99$. In the case of $\Delta t_1 = 5\Delta t_2$ (orange bars), the values are around $\lambda = 0.87$, $\lambda = 0.93$ and $\lambda = 0.99$. Note that for this example, the values of λ stay closer to $\lambda = 1.0$ than $\lambda = 0.0$, giving the wrong idea that the relaxation is not being useful, however, it has been verified that if the optimal relaxation parameter is not used, but rather a fixed value is employed, the number of iterations indeed increases.

5 CONCLUSIONS

In this work, the iterative coupling between the standard finite element method and the spectral finite element method for elastodynamic problems has been discussed. The fact that the subdomains are solved separately allows the use of distinct algorithms with respect to each subdomain. This is one of the major advantage of the proposed FEM-SFEM iterative coupling procedure. At the same time, the systems of equations to be solved are much smaller than the conventional coupled systems. The validity of the proposed method has been verified by means of a 2D numerical example. The lose of accuracy over the time, has been studied being able to cite some factors, it may be these, the pos-processing procedure used and the subparametric formulation for the SFEM.
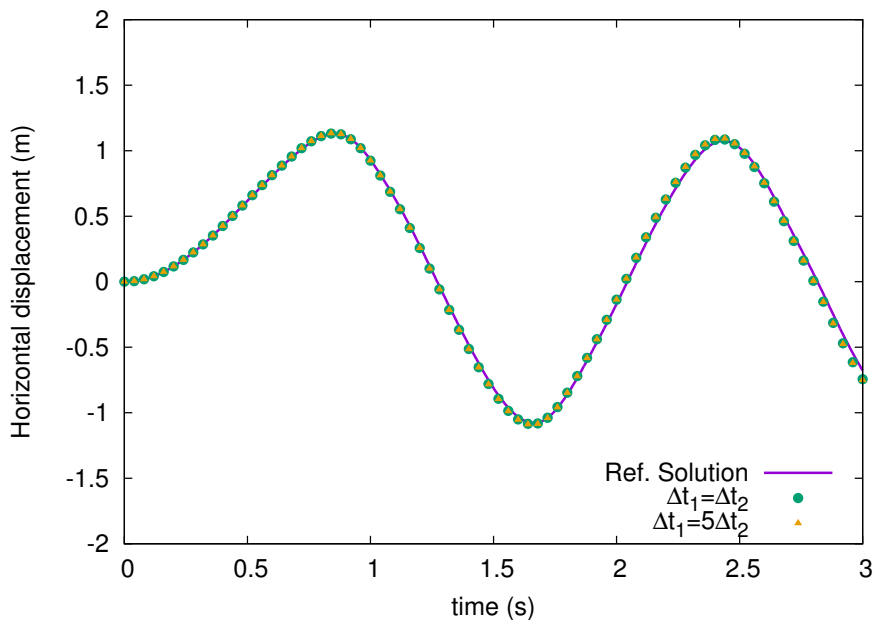
(a) Horizontal displacements
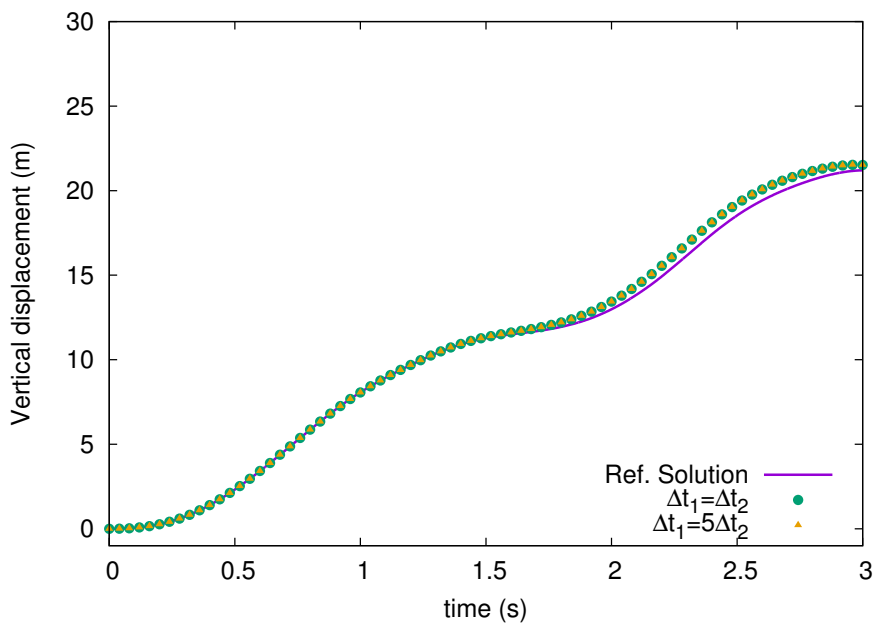
(b) Vertical displacements

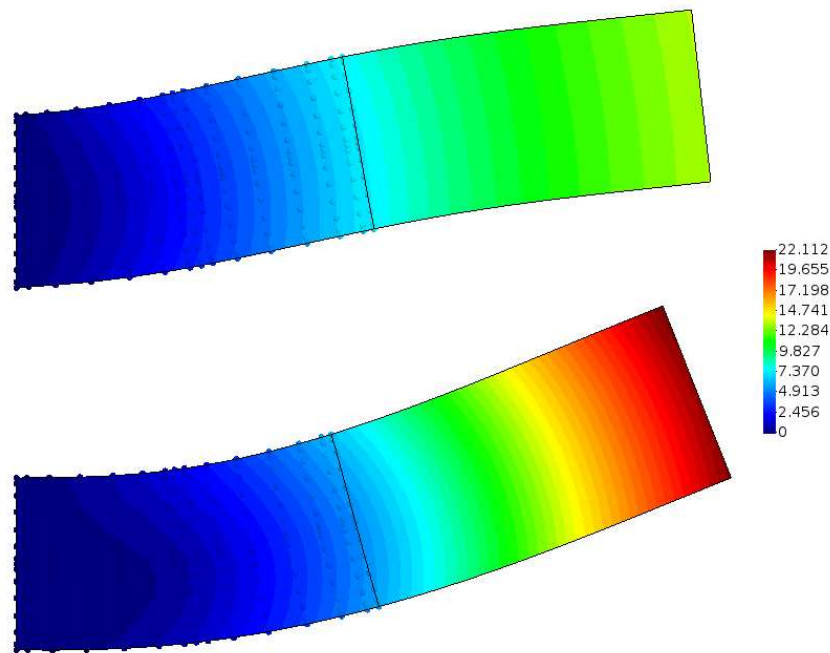Figure 4: Time-history results at the point A.

Figure 5: Snapshots of $\|\mathbf{u}\|$ at $t = 1.98$s and $t = 3$s, respectively, from the top to the bottom.

Acknowledgments

REFERENCES

Adams R. and Fournier J. *Sobolev Spaces*. Pure and Applied Mathematics. Elsevier Science, 2 edition, 2003.

Bathe K. *Finite element procedures*. Prentice-Hall, New Jersey, 1996.

Canuto C., Hussaini Y., Quarteroni A., and Zang T.A. *Spectral Methods: Fundamentals in Single Domains*. Springer, 2006.

Canuto C., Hussaini Y., Quarteroni A., and Zang T.A. *Spectral Methods: Evolution to Complex Geometries and Applications to Fluid Dynamics*. Springer, 2007.

Elleithy W., Al-Gahtani H., and El-Gebeily M. Iterative coupling of BE and FE methods in elastostatics. *Engineering Analysis with Boundary Elements*, 25(8):685–695, 2001.

Hughes T. *The finite element method: linear static and dynamic finite element analysis*. Dover Publications, New York, 2000.

Jr E.F., Santiago J., and Telles J. An iterative coupling between meshless methods to solve embedded crack problems. *Engineering Analysis with Boundary Elements*, 55:52 – 57, 2015.

Komatitsch D. and Tromp J. Introduction to the spectral element method for three-dimensional seismic wave propagation. *Geophysical Journal International*, 139(3):806–822, 1999.

Komatitsch D. and Vilotte J.P. The spectral element method: An efficient tool to simulate the seismic response of 2d and 3d geological structures. *Bulletin of the Seismological Society of America*, 88:368–392, 1998.

Szabo B. and Babuška I. *Finite Element Analysis*. Wiley, 1991.
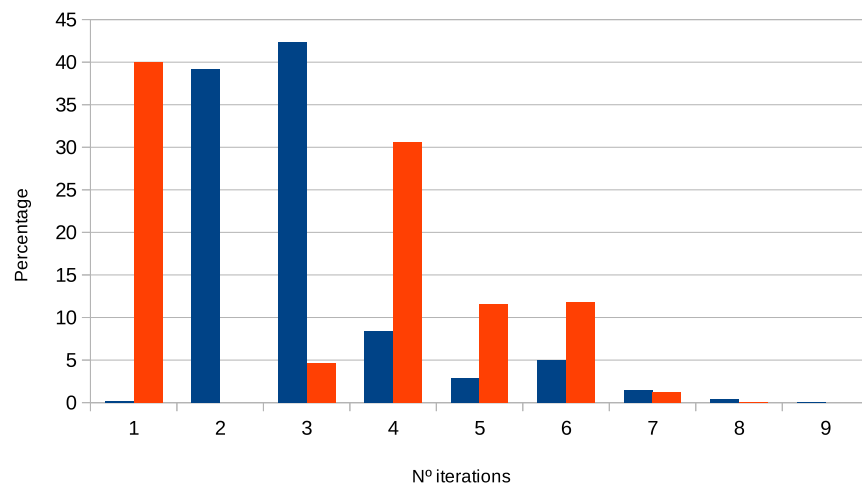
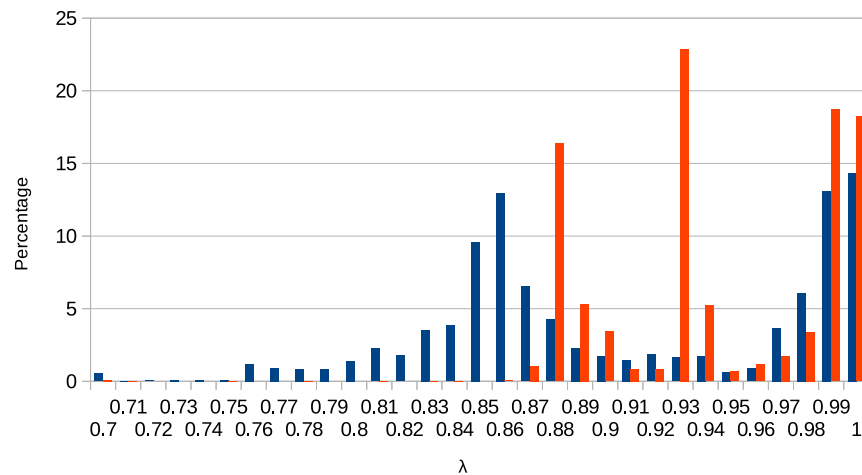(a) Distribution of the number of iterations at each time step.

(b) Distribution of the λ values at each iteration step.

Figure 6: Distribution of the number of iterations at each time step and λ values at each iteration step, the blue bars correspond to the case in which $\Delta t_1 = \Delta t_2$ and the orange bars to the $\Delta t_1 = 5\Delta t_2$.